THE JOURNAL OF PHYSICAL CHEMISTRY LETTERS
A JOURNAL OF THE AMERICAN CHEMICAL SOCIETY

pubs.acs.org/JPCL

Letter

Unravelling a Zigzag Pathway for Hot Carrier Collection with Graphene Electrode

Jin Zhang,*,# Hao Hong,# Jincan Zhang,# Chunchun Wu, Hailin Peng, Kaihui Liu,* and Sheng Meng*

Cite This: *J. Phys. Chem. Lett.* 2021, 12, 2886−2891

Read Online

ACCESS | Metrics & More | Article Recommendations | Supporting Information

ABSTRACT: The capture of photoexcited deep-band hot carriers, excited by photons with energies far above the bandgap, is of significant importance for photovoltaic and photoelectronic applications because it is directly related to the quantum efficiency of photon-to-electron conversion. By employing time-resolved photoluminescence and state-of-the-art time-domain density functional theory, we reveal that photoexcited hot carriers in organic−inorganic hybrid perovskites prefer a zigzag interfacial charge-transfer pathway, *i.e.*, the hot carriers transfer back and forth between $CH_3NH_3PbI_3$ and graphene electrode, before they reach a charge-separated state. Driven by quantum coherence and interlayer vibrational modes, this pathway at the semiconductor−graphene interface takes about 400 fs, much faster than the relaxation process within $CH_3NH_3PbI_3$ (several picoseconds). Our work provides new insight into the fundamental understanding and precise manipulation of hot carrier dynamics at the complex interfaces, paving the way for highly efficient photovoltaic and photoelectric device optimization.

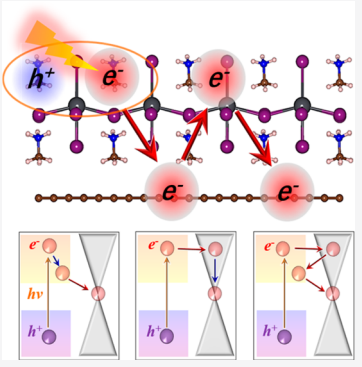

In conventional solar cells, hot charge carriers are generated by absorbing photons with energies larger than the bandgaps, which is generally followed by a quick cooling process; that is, the hot electrons relax to the band edges of semiconductors.[1−3] If the hot carriers can be captured within a time significantly shorter than the competing energy relaxation and loss processes, light-to-electricity conversion efficiency could be improved effectively. van der Waals (vdW) heterostructures provide a potential platform for investigating new physics and optoelectrical applications in hot carrier solar cells.[4−10] To achieve desirable performance in hot carrier devices based on vdW heterostructures, it is of central importance to understand and manipulate photoexcited hot carrier dynamics on an ultrafast time scale at the interfaces.[11−14]

Benefiting from the excellent optical properties, such as near-infrared to visible tunable bandgap, ultrahigh absorption, near-unity photoluminescence (PL) quantum yield, and nanosecond-scale long-lived photocarrier lifetime, organic−inorganic hybrid perovskites, *e.g.*, $CH_3NH_3PbI_3$ (termed $MAPbI_3$ hereafter), have emerged as ideal photoactive materials and been successfully used in light detection and emitters recently.[15−25] With two-dimensional (2D) graphene covered as an electrode, the perovskite−graphene heterostructures have gained substantial interest.[26−29] Several experimental works have reported interfacial carrier dynamics and high photoresponsivity on perovskite−graphene heterostructures.[27−30] Lee and coauthors demonstrated an intriguing photodetector consisting of $MAPbI_3$ and graphene, achieving a relatively high photoresponsivity and an effective quantum efficiency (5×10^4 % at an illumination power of 1 μW).[26] Recently, Hong *et al.* reported that graphene is an excellent carrier acceptor which extracts photoexcited hot carriers of $MAPbI_3$ crystal with interfacial deep-band charge transfer in less than 50 fs, significantly faster than the hot carrier relaxation or cooling process.[27] They focused on the ultrafast broadband charge collection at the clean graphene/organic−inorganic halide perovskite interfaces in an ultrashort time of ∼100 fs, with a high collection efficiency close to 99%. However, a comprehensive understanding of the dynamic process of photoexcited hot carriers at the semiconductor−graphene interfaces is still rare and in its early stages.

In this Letter, we utilize tunable two-color pump−probe spectroscopy, time-resolved PL spectroscopy, and the state-of-the-art time-domain density functional theory (DFT) to study the interlayer charge dynamics in model $CH_3NH_3PbI_3$/graphene (*i.e.*, $MAPbI_3$/graphene) heterostructure. Our results reveal that the ultrafast interlayer charge transfer in the heterostructure takes place on an order of ∼400 fs, in good agreement with experimental observations. Surprisingly, we find that photoexcited hot carriers in organic−inorganic hybrid perovskites prefer to undergo a zigzag pathway, *i.e.*, the hot electrons travel back and forth between $MAPbI_3$ and graphene. This work not only provides a new and complete physical

Received: January 30, 2021
Accepted: March 10, 2021
Published: March 16, 2021

picture into the hot carrier collection in heterostructures with graphene electrode on the atomic level but also sheds light on optimizing their performance toward future applications in high-speed photodetection and highly efficient light-harvesting materials.

In our experiments, chemical vapor deposition (CVD) grown graphene monolayer was cleanly transferred on a transmission electron microscopy (TEM) grid without polymer assistance (Figure S1 in the Supporting Information).[30] Then the clean interface of $MAPbI_3$/graphene was fabricated by directly growing single-crystal $MAPbI_3$ crystals on suspended graphene, as shown in Figure 1a. $MAPbI_3$ crystal

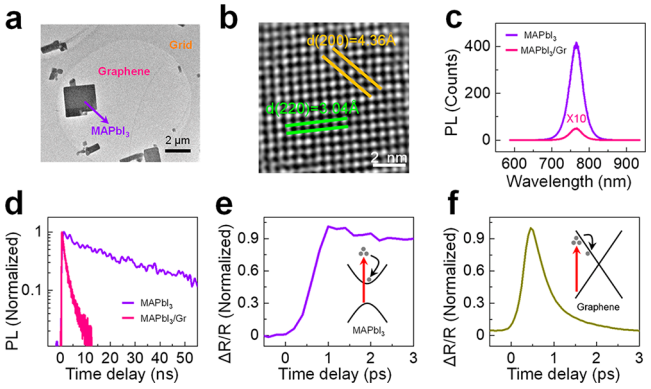

Figure 1. Experimental samples and pump−probe measurements of $MAPbI_3$/graphene heterostructure. (a) Transmission electron microscopy (TEM) image of the suspended $MAPbI_3$/graphene. (b) Representative aberration-corrected TEM images of the lattice structure of $MAPbI_3$. Typical lattice parameters are illustrated in the figure. The scale bar is 2 nm. (c) Photoluminescence (PL) spectra of $MAPbI_3$ with ($MAPbI_3$/Gr) and without graphene ($MAPbI_3$). (d) Time-resolved PL of pristine $MAPbI_3$ and $MAPbI_3$/Gr. With graphene underneath, the carrier lifetime of $MAPbI_3$ reduces dramatically from 25 to 1.3 ns. (e and f) The rise-up transient absorption spectrum of pristine $MAPbI_3$ (e) and graphene (f) under probe wavelength at 750 nm.

with a uniform thickness resides on the suspended graphene. The thickness of the perovskite is roughly determined to be 5−10 nm. Therefore, we can safely consider only the interfacial effect in our perovskite/graphene heterostructures. Figure 1b depicts the aberration-corrected atom-resolved TEM image of $MAPbI_3$, further proving the high crystallinity of our samples. No noticeable contaminants are observed around the $MAPbI_3$/graphene region, indicating the high cleanliness of the interface we fabricated. This clean interface promises strong interlayer coupling and an efficient interlayer charge-transfer process as discussed below.

In comparison with the pristine one, the PL intensity of $MAPbI_3$ is strongly quenched by nearly 2 orders of magnitude with graphene underneath (Figure 1c). In addition, the carrier lifetime reduces significantly (Figure 1d) on account of the new pathway of ultrafast carrier transfer at the interfaces. From our time-resolved PL experiments, pristine $MAPbI_3$ has a lifetime of ∼25 ns, while the lifetime of the $MAPbI_3$/graphene heterostructure is reduced significantly to ∼1.3 ns.

The carrier collection efficiency at the interface can be estimated from either the PL quench ($\eta_{PL} = 1 - \frac{I_{wGr}}{I_{w/oGr}} = 99\%$, where I_{wGr} and $I_{w/oGr}$ indicate the PL intensities of $MAPbI_3$/graphene and pristine $MAPbI_3$, respectively) or the lifetime decreases ($\eta_{PL} = 1 - \frac{\tau_{wGr}}{\tau_{w/oGr}} = 95\%$, where τ_{wGr} and $\tau_{w/oGr}$ indicate lifetimes of $MAPbI_3$/graphene and pristine $MAPbI_3$, respectively). These two different methods yield two different values, with the former one a little larger than the latter one. For the time-resolved PL experiment, the lifetime of cooling carriers at the band edge is measured. While it is a little complicated for the case of PL experiments, where deep-band carriers are excited and may directly transfer to graphene right after high-energy photons excitation. After high-energy excitation in perovskite, the carrier relaxation or cooling process inside the perovskite is very slow, with a typical time scale of ∼1 ps, as shown in the rise-up curve of Figure 1e (transient absorption signal with pump and probe wavelength at 400 and 750 nm, respectively), mainly because of phonon bottleneck effects.[20,21]

By contrast, hot carrier relaxation in graphene is relatively faster, with rise-up time of ∼0.4 ps (transient absorption signal with the same conditions as $MAPbI_3$) (Figure 1f). The transient absorption scales linearly as a function of pump fluence, implying no nonlinear effects are involved in measurement (Figure S2).[31−33] Therefore, the dynamic process of the photoexcited hot carriers at the semiconductor−graphene interfaces may be much more complicated and deserves a thorough time-domain atomistic description.

In Figure 2, we demonstrate three potential pathways involved in the photoinduced hot electron dynamics at the

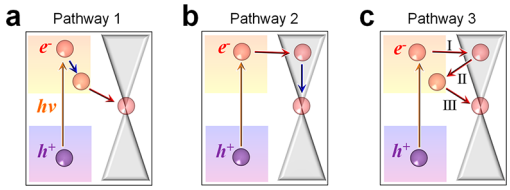

Figure 2. Schematic illustration of the photoinduced hot carrier dynamics at $MAPbI_3$/graphene heterostructure. (a) Pathway 1: photoexcited hot electron (e^-) in $MAPbI_3$ first relaxes to the band edge and then transfers to graphene. (b) Pathway 2: photoexcited hot electron in $MAPbI_3$ first transfers to graphene and then relaxes among graphene. (c) Pathway 3: photoexcited hot electron in $MAPbI_3$ first transfers to graphene across a zigzag pathway at semiconductor−graphene interfaces. I, II, and III indicate the separate steps of the pathway. Here, we consider the dynamics of photoexcited hot electrons while we observe similar results for hot holes (see the Supporting Information).

$MAPbI_3$/graphene heterojunction. In the beginning, optical excitation with a high-energy photon ($h\nu$ > bandgap of $MAPbI_3$) generates an electron (e^-) and hole (h^+) pair. Then, the hot carrier diffuses to graphene on account of the semiconductor−semimetal contacts. For pathway 1 (Figure 2a), the excited hot electron at $MAPbI_3$ first relaxes to the conduction band minimum (CBM) or the band edge of $MAPbI_3$ and then diffuses to graphene because of the band alignment. Pathway 2 is illustrated in Figure 2b, where the photoexcited hot carriers first transfer to the lowest-energy state of graphene and then relax to the Dirac point. Beyond them, strong interfacial interactions between $MAPbI_3$ and graphene may result in an alternative mechanism (pathway 3 in Figure 2c), where the hot electrons travel back and forth between the semiconductor and graphene in a zigzag pathway. The dominant pathway is determined by comparable time

https://dx.doi.org/10.1021/acs.jpclett.1c00347
J. Phys. Chem. Lett. 2021, 12, 2886−2891

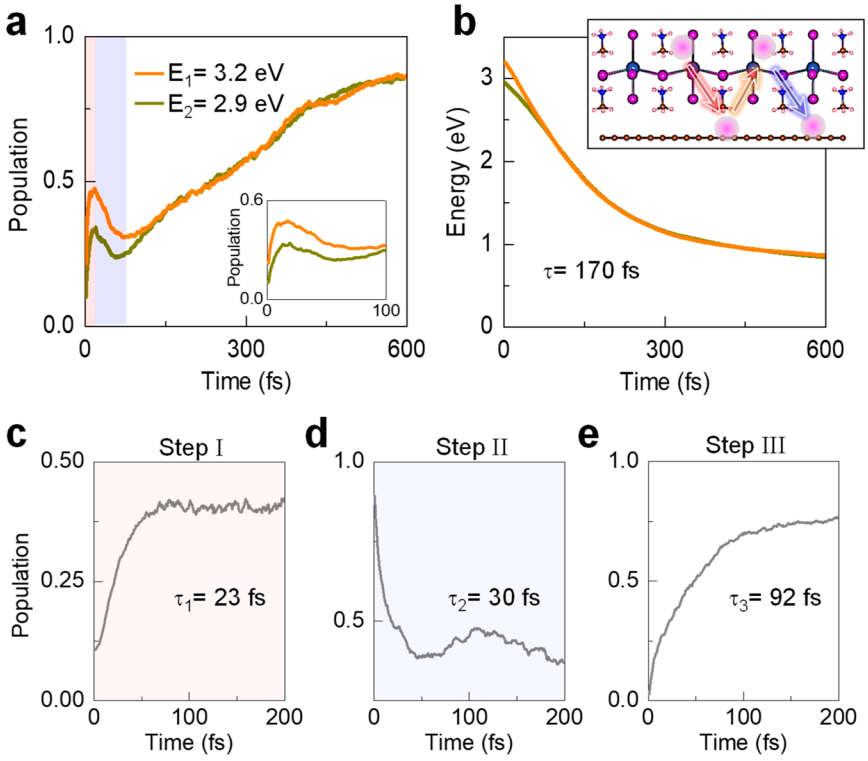

Figure 3. Hot carrier dynamics at $MAPbI_3$–graphene interfaces. (a) Population at $MAPbI_3$ of excited hot electron with initial photoexcited energies of 3.2 and 2.9 eV above the Fermi energy as a function of time upon optical excitation. For clarity, the inset shows the zoomed-in region from 0 to 100 fs. (b) Corresponding energy evolution of excited hot electrons. The inset cartoon exhibits the zigzag pathway in real space. Pathway 3 can be roughly divided into three substeps. (c) Evolution of the population of the hot electron from $MAPbI_3$ to graphene (step I). (d) Evolution of the population of the transferred hot electron state on graphene diffuses to $MAPbI_3$ on an ultrafast time scale of 30 fs (step II). (e) The excited electron at CBM transfers to graphene in 92 fs (step III). The time evolution data are fitted with exponential functions.

scales of interlayer charge transfer and intralayer hot carrier relaxation within the two individual components.

Considering our experimental observations as well as results from previous work,[26−29] we choose the vertical heterostructure of $MAPbI_3$ and graphene as a model to exploit the interfacial electronic properties and photoexcitation induced carrier dynamics in the semiconductor−semimetal interfaces. More information comes from the projected density of states (PDOS) of the heterostructure. The bandgap of $MAPbI_3$ in the heterostructure calculated with the Perdew−Burke−Ernzerhof (PBE) functional[34] is about 2.3 eV, and graphene is semimetallic with a zero bandgap (Figure S3). The CBM and valence band maximum (VBM) are both contributed mainly by electronic orbitals from $MAPbI_3$, reflecting a typical semiconductor−semimetal contact. One of the crucial parameters for charge diffusion at the interface is the band offsets at both CBM and VBM states. To validate our results, we compare the PDOS at the PBE level with that based on the HSE06 functional (Figure S4).[35] It is observed that the PBE functional is accurate enough to describe the spatial distribution of electronic states and the state couplings at $MAPbI_3$/graphene interfaces.

To investigate hot carrier dynamics,[36−44] we performed nonadiabatic analysis incorporating all orbitals with energies higher than the Fermi level of the heterostructure. Here, two typical hot electron states are selected: 3.2 and 2.9 eV above the Fermi level, respectively, and their dynamics are closely tracked. The hot electron states are selected according to the pump energy at 410 nm used in the pump−probe experiments discussed above. The spatial distributions of the CBM state in $MAPbI_3$ and the low-energy state above the Fermi level of graphene are also presented in Figure S5. The delocalization of the CBM state in $MAPbI_3$ is an indication of a relatively strong interfacial coupling.

To gain quantitative information, we integrate carrier populations on graphene orbitals at different times upon photoexcitation. The evolution of the localization is shown in Figure 3, where the population represents the fraction of the photoexcited charge density on the graphene sheet. At t = 0 fs, the two photoexcited states are mostly distributed on $MAPbI_3$, with 10% (for the state of 3.2 eV) and 20% (for the state of 2.9 eV) of the excited hot electrons diffusing to graphene in an ultrafast time scale (<20 fs for both states, Figure 3a). The population on graphene increases from 10% to 34% for the first charge diffusion process.

In the following, the hot electron diffuses back to $MAPbI_3$ and the population on graphene decreases to 23% at 50 fs. This process is not surprising because similar processes were observed in which a photoexcited hot carrier in graphene can inject into semiconductors (*i.e.*, WS_2) in about 25 fs, accompanied by a quantum yield as high as ∼50%.[8,45−47] Afterward, the hot electrons diffuse from $MAPbI_3$ to graphene with a large percentage (∼86%) within 600 fs. Simultaneously, the energy of the state decreases continuously from 2.9 to 1.0 eV upon photoexcitation (Figure 3b). Consequently, the time scale of the whole process is 400 fs with exponential fitting. The energy relaxation converges around 1 eV above the Fermi level (Figure 3b), because some states above the Fermi level of graphene are not included in the simulation because of the limit of the supercell.

https://dx.doi.org/10.1021/acs.jpclett.1c00347
J. Phys. Chem. Lett. 2021, 12, 2886−2891

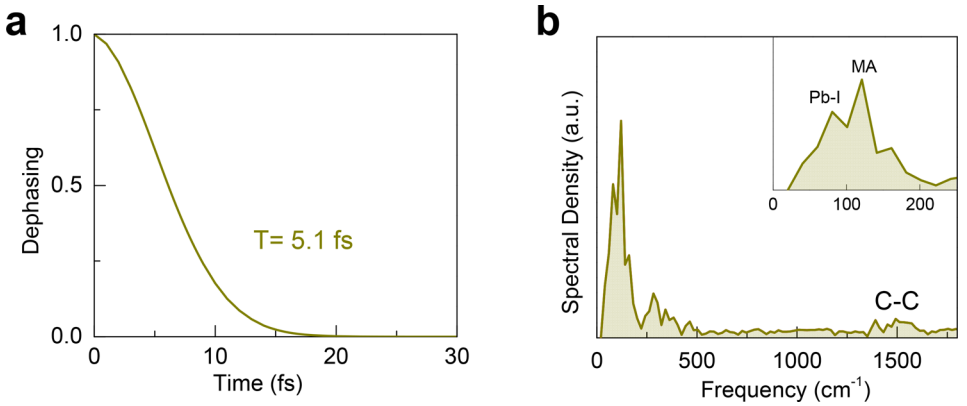

Figure 4. Phonon vibration facilitated hot electron transfer at $MAPbI_3$−graphene interfaces. (a) Pure-dephasing function of hot electron dynamics. (b) Spectral density of the phonon modes evolved in the dynamics: Pb−I bending, MA molecule rotation, and carbon−carbon stretching modes are crucial in the carrier dynamics. The inset presents the key phonon branches of $MAPbI_3$ involved in the charge dynamics.

By contrast, the charge population on graphene increases significantly in 23 fs (Figure 3a) for the excited state with the energy of 3.2 eV above the Fermi level. Then, this value drops to 30% at t = 75 fs. The total time scale of the photoexcited process is observed to be about 400 fs, accompanied by the energy decreasing continuously. These findings reveal there exists a new robust relaxation process (pathway 3) on a time scale of ∼400 fs, validating the experimentally observed ultrafast broadband charge transfer from $MAPbI_3$ to graphene.[27] Previous experiments have revealed that hot carrier relaxation in graphene takes place within ∼1 ps.[27] The result agrees well with our TDDFT calculations (the relaxation time is about 0.8 ps), as shown in Figure S6.

To have a clear understanding of the mechanism of the entangled processes, we separate the distinct processes by involving only relative states in the vicinity of the excited electron state. For step I (Figure 3c), the time scale of charge diffusion is about 23 fs from $MAPbI_3$ to graphene, in good agreement with experimental observation (<50 fs). Then in the following 30 fs, the electron-transfer process from graphene back to $MAPbI_3$ takes place (step II, as shown in Figure 3d).

On the other hand, there is an alternative cooling routine for the hot carriers: rapid electron−hole annihilation inside the semimetallic graphene with the assistance of effective electron−phonon and electron−electron scattering. This energy loss competes with charge separation and the dominant one determined by relative time scales. It is obtained that the relaxation time scale is ∼1 ps fs for the hot electron with the energy of ∼3.0 eV above the Fermi level in graphene, significantly slower than the interfacial charge-transfer process (30 fs). The lifetime is on the same order of magnitude with previous experimental studies (∼50 fs),[27] accounting for the strong interfacial interactions between $MAPbI_3$ and graphene and the assistance of interlayer phonon vibrations. For $MAPbI_3$, it is shown that the cooling process of hot carriers apparently takes a longer time (∼50 ps). Thus, the energy relaxation within both graphene and $MAPbI_3$ are much slower than the interface-assisted carrier dynamics, facilitating the novel pathway where hot electrons in the heterostructure would travel back and forth.

In order to accurately account for the band-edge carrier transfer, Figure 3e illustrates that the excited electrons at the CBM of $MAPbI_3$ further diffuse to graphene in 92 fs, in excellent accordance with the previous experimental result (110 fs).[27] These findings further rationalize the distinct charge dynamics for the band-edge electron (with the pump energy at 1.5 eV, 820 nm) and hot electron (pump energy of ∼3.0 eV, 410 nm) from $MAPbI_3$ to graphene using the PL excitation spectrum in experiments. Therefore, the results validate the novel and robust pathway 3, instead of the conventional decay pathways 1 and 2 at the vdW interfaces.

To further understand the peculiar pathway for photoexcited hot electron dynamics, more information coming from the effect of decoherence and phonons is analyzed in Figure 4a. Fourier transformation of the energy difference along the molecular dynamics permits a quantitative analysis of the crucial phonon vibrations mediated in the process (Figure 4b). We obtain that the Pb−I bond stretching mode (∼90 cm^{-1}) and the liberation of the organic cations ($CH_3NH_3^+$) at ∼120 cm^{-1} in perovskite−graphene heterostructure indeed plays a dominant role in ultrafast hot electron dynamics.[47,48] In addition, the frequency around 1500 cm^{-1} is attributed to carbon−carbon stretching modes in graphene. Therefore, phonon modes in both $MAPbI_3$ and graphene are involved in assisting the emergent zigzag-like hot electron-transfer route. This observation, together with strong coupling between $MAPbI_3$ and graphene layers, elucidates the mechanism of the newly discovered hot−electron collection channel.

In addition to the zigzag pathway, the photoexcited hot carriers may experience even more complicated pathways (*e.g.*, incorporating more states of graphene around the Fermi level and delicate interfacial charge-transfer processes). Thus, to fully understand the fate of photoexcited carriers, one should consider ultrafast intralayer/interlayer carrier scatterings, interfacial excitons, and charge-transfer processes at the semiconductor−graphene heterostructures. Besides, we also consider the dynamics of photoexcited hot electrons while we observe similar results for hot holes (Figure S7). The excitation light wavelength- and intensity-dependent TA measurement should be helpful for understanding the hot carrier-transfer process. We admit it is very difficult to directly prove the zigzag pathway for hot carrier collection by experiments. However, comprehensive comparison among different time scales for various processes validates the model shown in Figure 2. Beyond the graphene electrode, we envision the novel mechanism can be extended to other 2D metals, semimetals, surface states of topological insulators, and semiconductors if the interfacial interaction and atomic collective motions are strong enough to mediate the interlayer multiple charge transfer.

https://dx.doi.org/10.1021/acs.jpclett.1c00347
J. Phys. Chem. Lett. 2021, 12, 2886−2891

In summary, we demonstrate photoexcited hot carrier dynamics in heterostructures with graphene electrode using ultrafast transient absorption spectrum, time-resolves PL, and *ab initio* time-domain DFT simulations. We reveal that the strong interfacial interactions between $MAPbI_3$ and graphene result in a novel zigzag hot carrier cooling pathway, where the hot electron travels back and forth between semiconductors and graphene. Our calculations not only explain the experimentally observed ultrafast carrier dynamics upon photoexcitation at both band edges and deep bands but also present a new way to manipulate the hot carriers in semiconductor−graphene heterostructures in optoelectronic and photovoltaic applications. Therefore, improved device performance of hot carrier solar cells with graphene electrode may be achieved given that the photoexcited carriers in graphene can be extracted into electric circuits to minimize the loss in carrier conductors.

■ ASSOCIATED CONTENT

Supporting Information

The Supporting Information is available free of charge at https://pubs.acs.org/doi/10.1021/acs.jpclett.1c00347.

More details on photoinduced dynamics and methods (Figures S1−S7 and Note 1) (PDF)

■ AUTHOR INFORMATION

Corresponding Authors

Jin Zhang − *Beijing National Laboratory for Condensed Matter Physics and Institute of Physics, Chinese Academy of Sciences, Beijing 100190, P.R. China;* orcid.org/0000-0001-7830-3464; Email: jin.zhang@mpsd.mpg.de

Kaihui Liu − *State Key Laboratory for Mesoscopic Physics, School of Physics, Peking University, Beijing 100871, P.R. China; Collaborative Innovation Center of Quantum Matter, Beijing 100190, P.R. China;* orcid.org/0000-0002-8781-2495; Email: khliu@pku.edu.cn

Sheng Meng − *Beijing National Laboratory for Condensed Matter Physics and Institute of Physics, Chinese Academy of Sciences, Beijing 100190, P.R. China; Collaborative Innovation Center of Quantum Matter, Beijing 100190, P.R. China; Key Laboratory of Material Physics, School of Physics, Zhengzhou University, Zhengzhou 450052, P.R. China;* orcid.org/0000-0002-1553-1432; Email: smeng@iphy.ac.cn

Authors

Hao Hong − *State Key Laboratory for Mesoscopic Physics, School of Physics, Peking University, Beijing 100871, P.R. China*

Jincan Zhang − *College of Chemistry and Molecular Engineering, Academy for Advanced Interdisciplinary Studies, Peking University, Beijing 100871, P.R. China*

Chunchun Wu − *State Key Laboratory for Mesoscopic Physics, School of Physics, Peking University, Beijing 100871, P.R. China*

Hailin Peng − *College of Chemistry and Molecular Engineering, Academy for Advanced Interdisciplinary Studies, Peking University, Beijing 100871, P.R. China;* orcid.org/0000-0003-1569-0238

Complete contact information is available at: https://pubs.acs.org/10.1021/acs.jpclett.1c00347

Author Contributions

#J.Z., H.H., and J.Z. contributed equally to this work

Notes

The authors declare no competing financial interest.

■ ACKNOWLEDGMENTS

This work was supported by National Natural Science Foundation of China (Grant Nos. 11934003, 12025407, 11774396, 11474328, 51522201, 51991340, and 51991342), National Key Research and Development Program of China (Grant Nos. 2016YFA0300902 and 2016YFA0300903), and "Strategic Priority Research Program (B)" of Chinese Academy of Sciences (Grant No. XDB330301), Beijing Natural Science Foundation (JQ19004), and the China Postdoctoral Science Foundation (2020M680177).

■ REFERENCES

(1) Tisdale, W. A.; Williams, K. J.; Timp, B. A.; Norris, D. J.; Aydil, E. S.; Zhu, X. Y. Hot-electron transfer from semiconductor nanocrystals. *Science* **2010**, *328*, 1543−1547.

(2) Ross, R. T.; Nozik, A. J. Efficiency of hot-carrier solar energy converters. *J. Appl. Phys.* **1982**, *53*, 3813.

(3) Alivisatos, A. P. Semiconductor clusters, nanocrystals, and quantum dots. *Science* **1996**, *271*, 933.

(4) Geim, A. K.; Grigorieva, I. V. Van der Waals heterostructures. *Nature* **2013**, *499*, 419−425.

(5) Qiu, C.; Liu, F.; Xu, L.; Deng, B.; Xiao, M.; Si, J.; Lin, L.; Zhang, Z.; Wang, J.; Guo, H.; et al. Dirac-source field-effect transistors as energy-efficient, high-performance electronic switches. *Science* **2018**, *361*, 387−392.

(6) Massicotte, M.; Schmidt, P.; Vialla, F.; Schadler, K. G.; Reserbat-Plantey, A.; Watanabe, K.; Taniguchi, T.; Tielrooij, K. J.; Koppens, F. H. L. Picosecond photoresponse in van der Waals heterostructures. *Nat. Nanotechnol.* **2016**, *11*, 42−46.

(7) Yu, W. J.; Liu, Y.; Zhou, H. L.; Yin, A. X.; Li, Z.; Huang, Y.; Duan, X. F. Highly efficient gate-tunable photocurrent generation in vertical heterostructures of layered materials. *Nat. Nanotechnol.* **2013**, *8*, 952−958.

(8) Chen, Y.; Li, Y.; Zhao, Y.; Zhou, H.; Zhu, H. Highly efficient hot electron harvesting from graphene before electron-hole thermalization. *Sci. Adv.* **2019**, *5*, eaax9958.

(9) Wang, J.; Ball, J. M.; Barea, E. M.; Abate, A.; Alexander-Webber, J. A.; Huang, J.; Saliba, M.; Mora-Sero, I.; Bisquert, J.; Snaith, H. J.; et al. Low-temperature processed electron collection layers of graphene/TiO_2 nanocomposites in thin film perovskite solar cells. *Nano Lett.* **2014**, *14*, 724−730.

(10) Hong, X. P.; Kim, J.; Shi, S. F.; Zhang, Y.; Jin, C. H.; Sun, Y. H.; Tongay, S.; Wu, J. Q.; Zhang, Y. F.; Wang, F. Ultrafast charge transfer in atomically thin MoS_2/WS_2 heterostructures. *Nat. Nanotechnol.* **2014**, *9*, 682−686.

(11) Falke, S. M.; Rozzi, C. A.; Brida, D.; Maiuri, M.; Amato, M.; Sommer, E.; De Sio, A.; Rubio, A.; Cerullo, G.; Molinari, E.; et al. Coherent ultrafast charge transfer in an organic photovoltaic blend. *Science* **2014**, *344*, 1001−1005.

(12) Wang, H.; Bang, J.; Sun, Y.; Liang, L.; West, D.; Meunier, V.; Zhang, S. The role of collective motion in the ultrafast charge transfer in van der Waals heterostructures. *Nat. Commun.* **2016**, *7*, 11504.

(13) Qiao, L.; Fang, W.-H.; Long, R.; Prezhdo, O. V. Photoinduced dynamics of charge carriers in metal halide perovskites from an atomistic perspective. *J. Phys. Chem. Lett.* **2020**, *11* (17), 7066−7082.

(14) Wang, Y.; Fang, W.-H.; Long, R.; Prezhdo, O. V. Symmetry breaking at $MAPbI_3$ perovskite grain boundaries suppresses charge recombination: time-domain ab initio analysis. *J. Phys. Chem. Lett.* **2019**, *10* (7), 1617−1623.

(15) Xing, G. C.; Mathews, N.; Sun, S. Y.; Lim, S. S.; Lam, Y. M.; Gratzel, M.; Mhaisalkar, S.; Sum, T. C. Long-range balanced electron-

and hole-transport lengths in organic-inorganic $CH_3NH_3PbI_3$. *Science* **2013**, *342*, 344−347.
(16) Tong, C.-J.; Li, L.; Liu, L.-M.; Prezhdo, O. V. Synergy between ion migration and charge carrier recombination in metal-halide perovskites. *J. Am. Chem. Soc.* **2020**, *142* (6), 3060−3068.
(17) Zhou, H. P.; Chen, Q.; Li, G.; Luo, S.; Song, T. B.; Duan, H. S.; Hong, Z. R.; You, J. B.; Liu, Y. S.; Yang, Y. Interface engineering of highly efficient perovskite solar cells. *Science* **2014**, *345*, 542−546.
(18) Li, W.; Zhou, L.; Prezhdo, O. V.; Akimov, A. V. Spin−orbit interactions greatly accelerate nonradiative dynamics in lead halide perovskites. *ACS Energy Letters* **2018**, *3* (9), 2159−2166.
(19) Chu, W.; Saidi, W. A.; Prezhdo, O. V. Long-lived hot electron in a metallic particle for plasmonics and catalysis: Ab initio nonadiabatic molecular dynamics with machine learning. *ACS Nano* **2020**, *14* (8), 10608−10615.
(20) Zhu, H. M.; Miyata, K.; Fu, Y. P.; Wang, J.; Joshi, P. P.; Niesner, D.; Williams, K. W.; Jin, S.; Zhu, X. Y. Screening in crystalline liquids protects energetic carriers in hybrid perovskites. *Science* **2016**, *353*, 1409−1413.
(21) Jankowska, J.; Prezhdo, O. V. Ferroelectric alignment of organic cations inhibits nonradiative electron−hole recombination in hybrid perovskites: ab Initio nonadiabatic molecular dynamics. *J. Phys. Chem. Lett.* **2017**, *8* (4), 812−818.
(22) Lian, Z.; Yan, Q.; Lv, Q.; Wang, Y.; Liu, L.; Zhang, L.; Pan, S.; Li, Q.; Wang, L.; Sun, J.-L. High-performance planar-type photodetector on (100) facet of MAPbI 3 single crystal. *Sci. Rep.* **2015**, *5* (1), 16563.
(23) Shi, R.; Vasenko, A. S.; Long, R.; Prezhdo, O. V. Edge influence on charge carrier localization and lifetime in $CH_3NH_3PbBr_3$ perovskite: ab Initio quantum dynamics simulation. *J. Phys. Chem. Lett.* **2020**, *11* (21), 9100−9109.
(24) Marchioro, A.; Teuscher, J.; Friedrich, D.; Kunst, M.; van de Krol, R.; Moehl, T.; Gratzel, M.; Moser, J. E. Unravelling the mechanism of photoinduced charge transfer processes in lead iodide perovskite solar cells. *Nat. Photonics* **2014**, *8*, 250−255.
(25) Koppens, F.; Mueller, T.; Avouris, P.; Ferrari, A.; Vitiello, M.; Polini, M. Photodetectors based on graphene, other two dimensional materials and hybrid systems. *Nat. Nanotechnol.* **2014**, *9*, 780−793.
(26) Lee, Y.; Kwon, J.; Hwang, E.; Ra, C. H.; Yoo, W. J.; Ahn, J. H.; Park, J. H.; Cho, J. H. High-performance perovskite-graphene hybrid photodetector. *Adv. Mater.* **2015**, *27*, 41−46.
(27) Hong, H.; Zhang, J.; Zhang, J.; Qiao, R.; Yao, F.; Cheng, Y.; Wu, C.; Lin, L.; Jia, K.; Zhao, Y.; et al. Ultrafast broadband charge collection from clean graphene/$CH_3NH_3PbI_3$ interface. *J. Am. Chem. Soc.* **2018**, *140* (44), 14952−14957.
(28) Wang, Y. S.; Zhang, Y. P.; Lu, Y.; Xu, W. D.; Mu, H. R.; Chen, C. Y.; Qiao, H.; Song, J. C.; Li, S. J.; Sun, B. Q.; et al. Hybrid graphene-perovskite phototransistors with ultrahigh responsivity and gain. *Adv. Opt. Mater.* **2015**, *3*, 1389−1396.
(29) Tan, Z.; Wu, Y.; Hong, H.; Yin, J.; Zhang, J.; Lin, L.; Wang, M.; Sun, X.; Sun, L.; Huang, Y.; et al. Two-dimensional $(C_4H_9NH_3)_2PbBr_4$ perovskite crystals for high-performance photodetector. *J. Am. Chem. Soc.* **2016**, *138*, 16612−16615.
(30) Zhang, J.; Lin, L.; Sun, L.; Huang, Y.; Koh, A. L.; Dang, W.; Yin, J.; Wang, M.; Tan, C.; Li, T.; et al. Clean transfer of large graphene single crystals for high-intactness suspended membranes and liquid cells. *Adv. Mater.* **2017**, *29*, 1700639.
(31) Chu, W.; Zheng, Q.; Akimov, A. V.; Zhao, J.; Saidi, W. A.; Prezhdo, O. V. Accurate computation of nonadiabatic coupling with projector augmented-wave pseudopotentials. *J. Phys. Chem. Lett.* **2020**, *11* (23), 10073−10080.
(32) Tielrooij, K.; Song, J.; Jensen, S. A.; Centeno, A.; Pesquera, A.; Elorza, A. Z.; Bonn, M.; Levitov, L.; Koppens, F. Photoexcitation cascade and multiple hot-carrier generation in graphene. *Nat. Phys.* **2013**, *9* (4), 248−252.
(33) Tielrooij, K. J.; Piatkowski, L.; Massicotte, M.; Woessner, A.; Ma, Q.; Lee, Y.; Myhro, K. S.; Lau, C. N.; Jarillo-Herrero, P.; van Hulst, N. F.; et al. Generation of photovoltage in graphene on a femtosecond timescale through efficient carrier heating. *Nat. Nanotechnol.* **2015**, *10* (5), 437−443.
(34) Perdew, J. P.; Burke, K.; Ernzerhof, M. Generalized gradient approximation made simple. *Phys. Rev. Lett.* **1996**, *77*, 3865−3868.
(35) Heyd, J.; Scuseria, G. E.; Ernzerhof, M. Hybrid functionals based on a screened Coulomb potential. *J. Chem. Phys.* **2003**, *118*, 8207−8215.
(36) Blöchl, P. E. Projector augmented-wave method. *Phys. Rev. B: Condens. Matter Mater. Phys.* **1994**, *50*, 17953−17979.
(37) Kresse, G.; Joubert, D. From ultrasoft pseudopotentials to the projector augmented-wave method. *Phys. Rev. B: Condens. Matter Mater. Phys.* **1999**, *59* (3), 1758.
(38) Klimeš, J.; Bowler, D. R.; Michaelides, A. Van der Waals density functionals applied to solids. *Phys. Rev. B: Condens. Matter Mater. Phys.* **2011**, *83*, 195131.
(39) Klimeš, J.; Bowler, D. R.; Michaelides, A. Chemical accuracy for the van der Waals density functional. *J. Phys.: Cond. Mater.* **2009**, *22* (2), 022201.
(40) Tully, J. C. Molecular dynamics with electronic transitions. *J. Chem. Phys.* **1990**, *93*, 1061−1071.
(41) Craig, C. F.; Duncan, W. R.; Prezhdo, O. V. Trajectory surface hopping in the time-dependent Kohn-Sham approach for electron-nuclear dynamics. *Phys. Rev. Lett.* **2005**, *95*, 163001.
(42) Zhang, J.; Hong, H.; Zhang, J.; Fu, H.; You, P.; Lischner, J.; Liu, K.; Kaxiras, E.; Meng, S. New pathway for hot electron relaxation in two-dimensional heterostructures. *Nano Lett.* **2018**, *18*, 6057−6063.
(43) Parandekar, P. V.; Tully, J. C. Mixed quantum-classical equilibrium. *J. Chem. Phys.* **2005**, *122*, 094102.
(44) He, J.; Vasenko, A. S.; Long, R.; Prezhdo, O. V. Halide composition controls electron−hole recombination in cesium−lead halide perovskite quantum dots: a time domain ab initio study. *J. Phys. Chem. Lett.* **2018**, *9* (8), 1872−1879.
(45) Long, R.; English, N. J.; Prezhdo, O. V. Photo-induced charge separation across the graphene−TiO_2 interface is faster than energy losses: a time-domain ab initio analysis. *J. Am. Chem. Soc.* **2012**, *134*, 14238−14248.
(46) Manga, K. K.; Zhou, Y.; Yan, Y.; Loh, K. P. Multilayer hybrid films consisting of alternating graphene and titania nanosheets with ultrafast electron transfer and photoconversion properties. *Adv. Funct. Mater.* **2009**, *19*, 3638−3643.
(47) Quarti, C.; Grancini, G.; Mosconi, E.; Bruno, P.; Ball, J. M.; Lee, M. M.; Snaith, H. J.; Petrozza, A.; De Angelis, F. The Raman spectrum of the $CH_3NH_3PbI_3$ hybrid perovskite: interplay of theory and experiment. *J. Phys. Chem. Lett.* **2014**, *5*, 279−284.
(48) Chu, W.; Zheng, Q.; Prezhdo, O. V.; Zhao, J.; Saidi, W. A. Low-frequency lattice phonons in halide perovskites explain high defect tolerance toward electron-hole recombination. *Sci. Adv.* **2020**, *6*, eaaw7453.

https://dx.doi.org/10.1021/acs.jpclett.1c00347
J. Phys. Chem. Lett. 2021, 12, 2886−2891